



HAL
open science

A Six-Dof Epicyclic-Parallel Manipulator

Chao Chen, Thibault Gayral, Stéphane Caro, Damien Chablat, Guillaume Moroz, Sajeeva Abeywardena

► **To cite this version:**

Chao Chen, Thibault Gayral, Stéphane Caro, Damien Chablat, Guillaume Moroz, et al.. A Six-Dof Epicyclic-Parallel Manipulator. *Journal of Mechanisms and Robotics*, 2012, 4 (4), 10.1115/1.4007489 . hal-00684803

HAL Id: hal-00684803

<https://hal.science/hal-00684803v1>

Submitted on 3 Apr 2012

HAL is a multi-disciplinary open access archive for the deposit and dissemination of scientific research documents, whether they are published or not. The documents may come from teaching and research institutions in France or abroad, or from public or private research centers.

L'archive ouverte pluridisciplinaire **HAL**, est destinée au dépôt et à la diffusion de documents scientifiques de niveau recherche, publiés ou non, émanant des établissements d'enseignement et de recherche français ou étrangers, des laboratoires publics ou privés.

A Six-Dof Epicyclic-Parallel Manipulator

Chao Chen*

Department of Mechanical and Aerospace Engineering
Monash University
Victoria, Australia¹
Email: chao.chen@monash.edu

Thibault Gayral^{1,2}

Institut de Recherche en Communications et Cybernétique de Nantes
École Centrale de Nantes
Nantes, France²
Email: thibault.gayral@ens-cachan.org

Stéphane Caro², Damien Chablat², Guillaume Moroz²

Email: {stephane.caro; damien.chablat; guillaume.moroz}@ircsyn.ec-nantes.fr

Sajeeva Abeywardena¹

Email: sajeeva.abeywardena@monash.edu

A new six-dof epicyclic-parallel manipulator with all actuators allocated on the ground is introduced. It is shown that the system has a considerably simple kinematics relationship, with the complete direct and inverse kinematics analysis provided. Further, the first and second links of each leg can be driven independently by two motors. The serial and parallel singularities of the system are determined, with an interesting feature of the system being that the parallel singularity is independent of the position of the end-effector. The workspace of the manipulator is also analyzed with future applications in haptics in mind.

Keywords: parallel manipulator, epicyclic system, kinematics, workspace

1 Introduction

There are a large number of parallel manipulators which have been reported over the past three decades. They can be divided into three-dof, four-dof, five-dof and six-dof parallel manipulators [1–4]. In three-dof parallel manipulators, there are three-dof translational parallel manipulators [5–7], three-dof rotational parallel manipulators [8,9] and others [10,11]. Among the four-dof parallel manipulators, examples include the four-DOF four-URU parallel mechanism [12] and the McGill Schönflies-motion generator [13]. There are also five-dof parallel manipulators, such as 3T2R parallel manipulators [14,15]. For six-dof manipulators, the number of all

possible structures can be extremely large [16]. Six-legged six-dof parallel manipulators, such as the Gough-Stewart platform, have high stiffness and accuracy but suffer from a small workspace and limb interference. Three-legged six-dof manipulators were introduced to overcome this workspace limitation and do not suffer from the same limb interference as their six-legged counterparts [17]. However, to achieve six-dof with only three legs requires actuators to be mounted on the moving limbs, thus increasing the mass and inertia of the moving parts. A number of three-legged manipulators have been reported, such as [18–24], however, very few of them have all actuators allocated on the ground, [20,23,24] being some examples. Cleary and Brooks [20] used a differential drive system, Lee and Kim [23] used a gimbal mechanism and Monsarrat and Gosselin [24] used five-bar mechanisms as input drivers to allow for all actuators to be mounted on the base of a three-legged six-dof parallel mechanism.

This paper proposes a new design of a six-dof three-legged parallel manipulator with all base mounted actuators, the Monash Epicyclic-Parallel Manipulator (MEPaM). The design is achieved by utilising the advantages of two-dof planetary belt systems, namely transmitting power from a base-mounted actuator to a moving joint. By mounting actuators on the base, the mass and inertia of the moving links is greatly reduced resulting in a lightweight six-dof parallel manipulator.

This paper is organized as follows. Section 2 describes the concept design and provides solutions to the direct and

*All correspondence should be addressed to this author

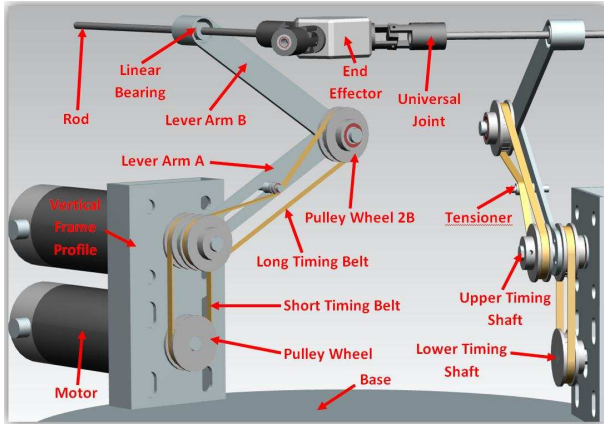


Fig. 1. Virtual model of MEPaM (one leg is hidden for clarity)

inverse kinematics problems for the manipulator. The singularities of MEPaM are analysed in Section 3 and its workspace in Section 4. Finally, the first prototype and future applications of MEPaM are briefly discussed in Section 5.

2 Concept Design

The proposed six-dof parallel manipulator is illustrated in Fig. 1. There are three identical planetary-belt mechanisms, each having two-dof driven by two motors. The driving planes of the planetary systems form an equilateral triangle. The output of the subsystem is an arm attached to the planet, Lever Arm B. There is a cylindrical joint attached to an end of this arm, perpendicular to the corresponding driving plane. A triangular end-effector is connected to the three cylindrical joints via universal joints on its vertices.

The planetary belt-pulley system shown in Fig. 1 has a transmission ratio of 1, providing two-dof movement in a flat plane. The carrier, Lever Arm A, is driven by a lower motor via a short stiff belt, while the sun pulley is driven by the upper motor. This motion is transmitted to the planet pulley via a long stiff belt. The arm attached to the planet is therefore driven by these two motors and hence, the end-effector controlled by six motors.

2.1 Direct Kinematics

The problem of direct kinematics is to find the position and orientation of the end effector, given the position of all the controlled joints. There are six motors all together, so there are six angles to be specified, i.e. θ_{1a} , θ_{1b} , θ_{2a} , θ_{2b} , θ_{3a} and θ_{3b} . There are also three pairs of angles indicating the angles of the carrier and the planet denoted θ_{1c} , θ_{1p} , θ_{2c} , θ_{2p} , θ_{3c} and θ_{3p} . Fig. 2 shows the planetary belt-pulley transmission. According to Fig. 2, we have

$$A_{1x} = w + d_1 \cos \theta_{1c} + d_2 \cos \theta_{1p} \quad (1a)$$

$$A_{1z} = w + d_1 \sin \theta_{1c} + d_2 \sin \theta_{1p} \quad (1b)$$

where (w, w) is the Cartesian coordinate vector of the sun cen-

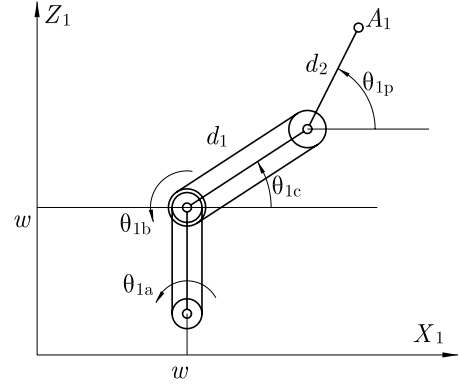


Fig. 2. The belt-pulley transmission

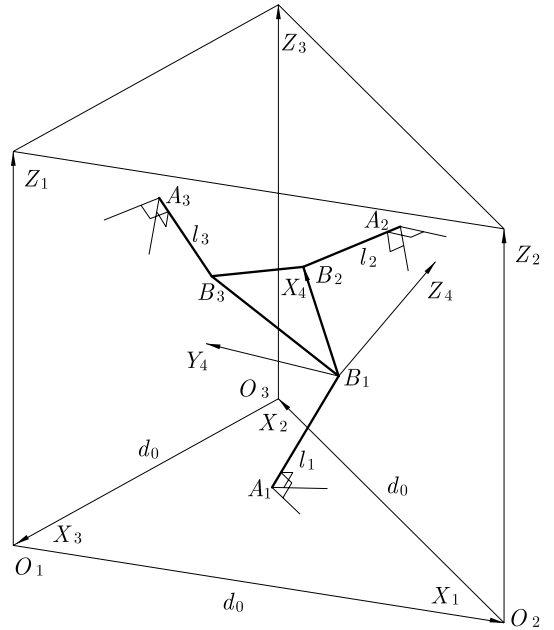


Fig. 3. The end-effector connecting to A_1 , A_2 , and A_3

ter. Due to the planetary transmission, we have

$$\frac{\theta_{1b} - \theta_{1c}}{\theta_{1p} - \theta_{1c}} = 1 \quad (2)$$

Given a proper reference for θ_{1a} , we should have $\theta_{1c} = \theta_{1a}$. Therefore, Eqn. (2) can be written as $\theta_{1p} = \theta_{1b}$. This indicates that the motions of the carrier and the planet can be independently controlled by Motor 1A and Motor 1B, respectively. Eqns. (1) can be further written as

$$A_{ix} = w + d_1 \cos \theta_{ia} + d_2 \cos \theta_{ib} \quad (3a)$$

$$A_{iz} = w + d_1 \sin \theta_{ia} + d_2 \sin \theta_{ib} \quad (3b)$$

for $i = 1, 2, 3$.

With the actuators locked, the manipulator has a structure equivalent to that of the 3PS manipulator analysed by Parenti-Castelli and Innocenti [25], the difference being that

MEPaM is a six-dof manipulator with six actuators allocated on the base as opposed to the three-dof, three actuator 3PS manipulator. Nevertheless, it is still an important task to formulate the steps necessary to find the strokes of the three cylindrical joints, l_i for $i = 1, 2, 3$, upon the geometric constraints on the triangular platform. The frame assignment for the driving planes as well as the end-effector are shown in Fig. 3. Three fixed frames, \mathcal{F}_1 , \mathcal{F}_2 and \mathcal{F}_3 , are attached to the base in an equilateral triangle formation, while a moving frame \mathcal{F}_4 is attached to the triangular end effector of side length d_3 . \mathbf{a}_i and \mathbf{b}_i are the Cartesian coordinate vectors of points A_i and B_i , respectively. An upper-left index is used to indicate in which frame the vector is expressed. Since each cylindrical joint is perpendicular to the corresponding plane, we have

$${}^1\mathbf{b}_1 = \begin{bmatrix} A_{1x} \\ l_1 \\ A_{1z} \end{bmatrix}, \quad {}^2\mathbf{b}_2 = \begin{bmatrix} A_{2x} \\ l_2 \\ A_{2z} \end{bmatrix}, \quad {}^3\mathbf{b}_3 = \begin{bmatrix} A_{3x} \\ l_3 \\ A_{3z} \end{bmatrix} \quad (4)$$

From Fig. 3, the transformation matrices between frames \mathcal{F}_1 , \mathcal{F}_2 and \mathcal{F}_3 are given by

$${}^1_2\mathbf{T} = {}^2_3\mathbf{T} = {}^3_1\mathbf{T} = \begin{bmatrix} \cos(2\pi/3) & -\sin(2\pi/3) & 0 & d_0 \\ \sin(2\pi/3) & \cos(2\pi/3) & 0 & 0 \\ 0 & 0 & 1 & 0 \\ 0 & 0 & 0 & 1 \end{bmatrix}$$

Hence, the positions of all the vertices can be transformed into \mathcal{F}_1 , i.e.,

$${}^1\mathbf{b}_i = {}^1_1\mathbf{T} {}^i\mathbf{b}_i \quad (5)$$

for $i = 2, 3$. The geometric constraints on the device are given by

$$\|{}^1\mathbf{b}_i - {}^1\mathbf{b}_j\|^2 = d_3^2 \quad (6)$$

for $i = 1, 2, 3$ and $j = i + 1 \pmod{3}$.

The constraint equations, Eqns. (6), contain only three variables l_i , $i = 1, 2, 3$, and can be further written in the form:

$$D_2 l_2^2 + D_1 l_2 + D_0 = 0 \quad (7a)$$

$$E_2 l_3^2 + E_1 l_3 + E_0 = 0 \quad (7b)$$

$$F_2 l_3^2 + F_1 l_3 + F_0 = 0 \quad (7c)$$

where D_j, E_j, F_j ($j = 0, 1, 2$) are functions of l_1, l_2 and l_1 respectively, as well as d_3, A_{ix} and A_{iz} ($i = 1, 2, 3$).

By means of dialytic elimination [26], the system of equations (7) can be reduced to a univariate polynomial of

order four in the variable l_1 :

$$G_4 l_1^4 + G_3 l_1^3 + G_2 l_1^2 + G_1 l_1 + G_0 = 0 \quad (8)$$

where the coefficients G_k ($k = 0 \dots 4$) are given in the Appendix. Note that for the 3PS structure analysed by Parenti-Castelli and Innocenti [25], the univariate polynomial was of order eight. Once Eqn. (8) has been solved for l_1 , substitution of the result into Eqns. (7) will allow for determination of l_2 and l_3 . The complexity of Eqns. (6) is relatively low as compared to the direct kinematics problem in most six-dof parallel manipulators. Solutions of l_i for $i = 1, 2, 3$ can be used to evaluate the position and orientation of the end-effector. The position of the end-effector is simply the origin of \mathcal{F}_4 , given by ${}^1\mathbf{b}_1 = [A_{1x} \quad l_1 \quad A_{1z}]^T$. The orientation of the end-effector is given by

$${}^1_4\mathbf{Q} = [\mathbf{i} \quad \mathbf{j} \quad \mathbf{k}]$$

where

$$\begin{aligned} \mathbf{i} &= \frac{{}^1\mathbf{b}_2 - {}^1\mathbf{b}_1}{\|{}^1\mathbf{b}_2 - {}^1\mathbf{b}_1\|} \\ \mathbf{j} &= \frac{({}^1\mathbf{b}_3 - {}^1\mathbf{b}_1) - \mathbf{i}\mathbf{i}^T({}^1\mathbf{b}_3 - {}^1\mathbf{b}_1)}{\|({}^1\mathbf{b}_3 - {}^1\mathbf{b}_1) - \mathbf{i}\mathbf{i}^T({}^1\mathbf{b}_3 - {}^1\mathbf{b}_1)\|} \\ \mathbf{k} &= \mathbf{i} \times \mathbf{j} \end{aligned} \quad (9)$$

Therefore, the direct kinematics of MEPaM is solved.

2.2 Inverse Kinematics

The problem of inverse kinematics is to find the six input angles, given the position and orientation of the end-effector, i.e. ${}^1\mathbf{o}_4$ and ${}^1_4\mathbf{Q}$. The Cartesian coordinate vectors of the vertices of the moving platform, denoted B_1, B_2 and B_3 , are given by:

$${}^1\mathbf{b}_i = {}^1\mathbf{o}_4 + {}^1_4\mathbf{Q} {}^4\mathbf{b}_i \quad (10)$$

for $i = 1, 2, 3$, where ${}^4\mathbf{b}_1 = [0 \quad 0 \quad 0]^T$, ${}^4\mathbf{b}_2 = [d_3 \quad 0 \quad 0]^T$, and ${}^4\mathbf{b}_3 = [d_3/2 \quad \sqrt{3}d_3/2 \quad 0]^T$.

Upon Eqns. (3), we can readily find the motor inputs, i.e. θ_{ia} and θ_{ib} for $i = 1, 2, 3$. First, the Eqns. (3) are re-written as

$$\alpha_{i1} - d_1 \cos \theta_{ia} = d_2 \cos \theta_{ib} \quad (11a)$$

$$\alpha_{i2} - d_1 \sin \theta_{ia} = d_2 \sin \theta_{ib} \quad (11b)$$

where $\alpha_{i1} = A_{ix} - w$ and $\alpha_{i2} = A_{iz} - w$ for $i = 1, 2, 3$. Then A_{ix} and A_{iz} are found from Eqn. (4) which requires substituting Eqn. (10) into Eqn. (5) to solve for the component values. Squaring Eqns. (11) and adding the resultants yields a single

equation in one variable for each θ_{ia} :

$$\beta_i - 2d_1\alpha_{i1}\cos\theta_{ia} - 2d_2\alpha_{i2}\sin\theta_{ia} = 0 \quad (12)$$

where $\beta_i = \alpha_{i1}^2 + \alpha_{i2}^2 + d_1^2 - d_2^2$ for $i = 1, 2, 3$. By using the half angle formulae, eq. (12) becomes a quadratic equation in $\tan(\theta_{ia}/2)$ with solution

$$\tan\frac{\theta_{ia}}{2} = \frac{4d_1\alpha_{i2} \pm \sqrt{16d_1^2(\alpha_{i1}^2 + \alpha_{i2}^2) - 4\beta_i^2}}{2(\beta_i + 2d_1\alpha_{i1})} \quad (13)$$

for $i = 1, 2, 3$. Knowing θ_{ia} allows for the calculation of θ_{ib} with the use of eqs. (11):

$$\tan\theta_{ib} = \frac{\alpha_{i2} - d_1\sin\theta_{ia}}{\alpha_{i1} - d_1\cos\theta_{ia}} \quad (14)$$

for $i = 1, 2, 3$. Hence, the inverse kinematics problem has been solved. From Eqn. (13), it can be seen that there are two possible solutions for each arm which indicates that generally there are two possible configurations (working modes) of each arm for any pose of the end-effector.

3 Singularity Analysis

The singularities of the manipulator can be found from the determinant of the serial and parallel Jacobian matrices, \mathbf{J}_S and \mathbf{J}_P , respectively [27]. The Jacobian matrices satisfy the following relationship:

$$\mathbf{J}_S \dot{\Theta} = \mathbf{J}_P \mathbf{t} \quad (15)$$

where $\dot{\Theta}$ is the vector of active joint rates and \mathbf{t} is the twist of the moving platform.

3.1 Serial Singularities

The serial Jacobian matrix can be obtained by differentiating Eqn. (3) with respect to time, which yields:

$$\mathbf{J}_S = \begin{bmatrix} \mathbf{J}_1 & \mathbf{0}_{2 \times 2} & \mathbf{0}_{2 \times 2} \\ \mathbf{0}_{2 \times 2} & \mathbf{J}_2 & \mathbf{0}_{2 \times 2} \\ \mathbf{0}_{2 \times 2} & \mathbf{0}_{2 \times 2} & \mathbf{J}_3 \end{bmatrix}$$

where

$$\mathbf{J}_i = \begin{bmatrix} -d_1 \sin\theta_{ia} & -d_2 \sin\theta_{ib} \\ d_1 \cos\theta_{ia} & d_2 \cos\theta_{ib} \end{bmatrix}$$

The serial singularities occur when the determinant of

\mathbf{J}_S is null, namely,

$$-(d_1 d_2)^3 \prod_{i=1}^3 \sin(\theta_{ia} - \theta_{ib}) = 0$$

Hence, the serial singularities occur when

$$\theta_{ia} - \theta_{ib} = 0 \text{ or } \pi$$

In such configurations, the arms of the planetary gear systems are either fully extended or folded. This result is as expected, since when the arms are in such an arrangement the moving platform can no longer move in the direction of the arms and thus loses one dof.

3.2 Parallel Singularities

Whilst the parallel singularities of the manipulator can be determined from the parallel Jacobian matrix, an alternative means is able to provide geometric insight into their meaning. A geometric condition for the manipulator singularities is obtained by means of Grassmann-Cayley Algebra with the actuation singularities being able to be plotted in the manipulator's orientation workspace.

Grassmann-Cayley Algebra (GCA), also known as exterior algebra, was developed by H. Grassmann as a calculus for linear varieties operating on *extensors* with the *join* and *meet* operators. The latter are associated with the *span* and *intersection* of vector spaces of extensors. Extensors are symbolically denoted by Plücker coordinates of lines and characterized by their *step*. In the four-dimensional vector space V associated with the three-dimensional projective space P^3 , extensors of step 1, 2 and 3 represent points, lines and planes, respectively. They are also associated with subspaces of V , of dimension 1, 2 and 3, respectively. Points are represented with their homogeneous coordinates, while lines and planes are represented with their Plücker coordinates. The notion of extensor makes it possible to work at the symbolic level and therefore, to produce coordinate-free algebraic expressions for the geometric singularity conditions of spatial parallel manipulators (PMs). For further details on GCA, the reader is referred to [28–32].

3.2.1 Wrench System of MEPaM

The actuated joints of MEPaM are the first two revolute joints of each leg. The actuation wrench $\hat{\tau}_{01}^i$ corresponding to the first revolute joint of the i th leg is reciprocal to all the twists of the leg, but to the twist associated with its first revolute joint. Likewise, the actuation wrench $\hat{\tau}_{02}^i$ corresponding to the second revolute joint of the i th leg is reciprocal to all the twists of the leg, but to the twist associated with its second revolute joint. As a result,

$$\hat{\tau}_{01}^1 = \begin{bmatrix} \mathbf{u} \\ \mathbf{b}_1 \times \mathbf{u} \end{bmatrix}, \hat{\tau}_{01}^2 = \begin{bmatrix} \mathbf{v} \\ \mathbf{b}_2 \times \mathbf{v} \end{bmatrix}, \hat{\tau}_{01}^3 = \begin{bmatrix} \mathbf{w} \\ \mathbf{b}_3 \times \mathbf{w} \end{bmatrix} \quad (16)$$

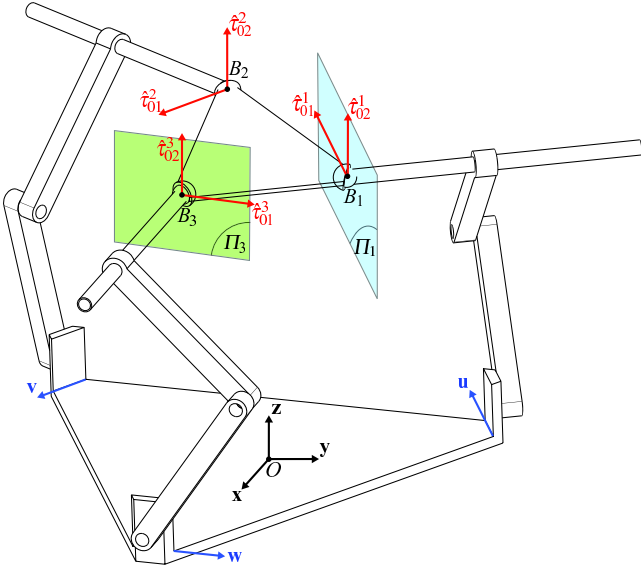


Fig. 4. The actuation forces applied on the moving platform of MEPaM

and

$$\hat{\tau}_{02}^1 = \begin{bmatrix} \mathbf{z} \\ \mathbf{b}_1 \times \mathbf{z} \end{bmatrix}, \hat{\tau}_{02}^2 = \begin{bmatrix} \mathbf{z} \\ \mathbf{b}_2 \times \mathbf{z} \end{bmatrix}, \hat{\tau}_{02}^3 = \begin{bmatrix} \mathbf{z} \\ \mathbf{b}_3 \times \mathbf{z} \end{bmatrix} \quad (17)$$

In a non-singular configuration, the six actuation wrenches $\hat{\tau}_{01}^1, \hat{\tau}_{02}^1, \hat{\tau}_{01}^2, \hat{\tau}_{02}^2, \hat{\tau}_{01}^3$ and $\hat{\tau}_{02}^3$, which are illustrated in Fig. 4, span the actuation wrench system of MEPaM. As MEPaM does not have any constraint wrenches, its global wrench system amounts to its actuation wrench, namely,

$$\mathcal{W}_{MEPaM} = \text{span}(\hat{\tau}_{01}^1, \hat{\tau}_{02}^1, \hat{\tau}_{01}^2, \hat{\tau}_{02}^2, \hat{\tau}_{01}^3, \hat{\tau}_{02}^3) \quad (18)$$

The legs of MEPaM apply six actuation forces to its moving-platform. Its global wrench system is a six-system. A parallel singularity occurs when the wrenches in the six-system become linearly dependent and span a k -system with $k < 6$.

3.2.2 Wrench Graph of MEPaM in P^3

The six actuation wrenches $\hat{\tau}_{01}^1, \hat{\tau}_{02}^1, \hat{\tau}_{01}^2, \hat{\tau}_{02}^2, \hat{\tau}_{01}^3$ and $\hat{\tau}_{02}^3$ form a basis of the global wrench system \mathcal{W}_{MEPaM} . Those wrenches are represented by six finite lines in P^3 . To obtain the six extensors of MEPaM's superbracket, twelve projective points on the six projective lines need to be selected, i.e. two points on each line. The extensor of a finite line can be represented by either two distinct finite points or one finite point and one infinite point since any finite line has one point at infinity corresponding to its direction.

B_1, B_2 and B_3 are the intersection points of $\hat{\tau}_{01}^1$ and $\hat{\tau}_{02}^1$, $\hat{\tau}_{01}^2$ and $\hat{\tau}_{02}^2$, $\hat{\tau}_{01}^3$ and $\hat{\tau}_{02}^3$, respectively. Let $\mathbf{b}_1, \mathbf{b}_2$ and \mathbf{b}_3 denote the homogeneous coordinates of points B_1, B_2 and B_3 , respectively. As shown in Fig. 4, $\hat{\tau}_{02}^1, \hat{\tau}_{02}^2$ and $\hat{\tau}_{02}^3$ are parallel and intersect at the infinite plane Π_∞ at point $\underline{\mathbf{z}} = (\mathbf{z}, 0)^T$, which corresponds to the Z direction. $\hat{\tau}_{01}^1$ is along vector \mathbf{u}

and intersects at the infinite plane Π_∞ at point $\underline{\mathbf{u}} = (\mathbf{u}, 0)^T$. $\hat{\tau}_{01}^2$ is along vector \mathbf{v} and intersects at the infinite plane Π_∞ at point $\underline{\mathbf{v}} = (\mathbf{v}, 0)^T$. $\hat{\tau}_{01}^3$ is along vector \mathbf{w} and intersects at the infinite plane Π_∞ at point $\underline{\mathbf{w}} = (\mathbf{w}, 0)^T$. Let $\underline{\mathbf{x}} = (\mathbf{x}, 0)^T$ and $\underline{\mathbf{y}} = (\mathbf{y}, 0)^T$. As vectors \mathbf{u}, \mathbf{v} and \mathbf{w} are normal to vector \mathbf{z} , points $\underline{\mathbf{u}}, \underline{\mathbf{v}}, \underline{\mathbf{x}}$ and $\underline{\mathbf{y}}$ are aligned at the infinite plane Π_∞ .

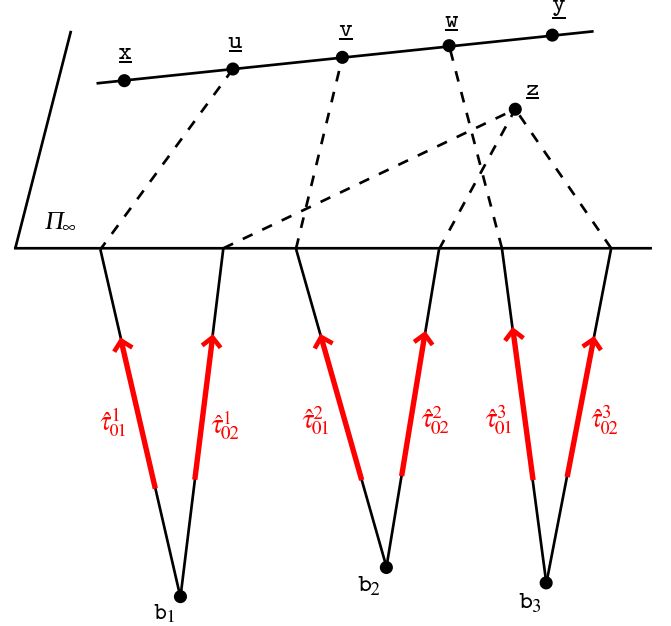


Fig. 5. The wrench graph of MEPaM

The actuation forces can be expressed by means of the six projective points $\mathbf{b}_1, \mathbf{b}_2, \mathbf{b}_3, \underline{\mathbf{u}}, \underline{\mathbf{v}}$ and $\underline{\mathbf{w}}$ as follows: $\hat{\tau}_{01}^1 \equiv \mathbf{b}_1 \underline{\mathbf{u}}$, $\hat{\tau}_{02}^1 \equiv \mathbf{b}_1 \underline{\mathbf{z}}$, $\hat{\tau}_{01}^2 \equiv \mathbf{b}_2 \underline{\mathbf{v}}$, $\hat{\tau}_{02}^2 \equiv \mathbf{b}_2 \underline{\mathbf{z}}$, $\hat{\tau}_{01}^3 \equiv \mathbf{b}_3 \underline{\mathbf{w}}$ and $\hat{\tau}_{02}^3 \equiv \mathbf{b}_3 \underline{\mathbf{z}}$. As a result, the wrench graph of MEPaM is as shown in Fig. 5.

3.2.3 Superbracket of MEPaM

The rows of the backward Jacobian matrix of a parallel manipulator are the Plücker coordinates of six lines in P^3 . The superjoin of these six vectors in P^5 corresponds to the determinant of their six Plücker coordinate vectors up to a scalar multiple, which is the superbracket in GCA $\Lambda(V^{(2)})$ [33]. Thus, a singularity occurs when these six Plücker coordinate vectors are dependent, which is equivalent to a superbracket equal to zero.

From Fig. 5, MEPaM's superbracket S_{MEPaM} can be expressed as follows:

$$S_{MEPaM} = [\mathbf{b}_1 \underline{\mathbf{u}} \mathbf{b}_1 \underline{\mathbf{z}} \mathbf{b}_2 \underline{\mathbf{v}} \mathbf{b}_2 \underline{\mathbf{z}} \mathbf{b}_3 \underline{\mathbf{w}} \mathbf{b}_3 \underline{\mathbf{z}}] \quad (19)$$

This expression can be developed into a linear combination of 24 bracket monomials [16, 34], each one being the product of three brackets of four projective points. A simplified expression of MEPaM's superbracket was obtained by means of a graphical user interface recently developed in the frame-

work of the ANR SIROPA project [35], namely,

$$S_{MEPaM} = [b_1 \ b_2 \ \underline{z} \ b_3] \left([b_1 \ \underline{u} \ \underline{z} \ b_2] [\underline{v} \ \underline{w} \ b_3 \ \underline{z}] - [b_1 \ \underline{u} \ \underline{z} \ \underline{v}] [b_2 \ \underline{w} \ b_3 \ \underline{z}] \right) \quad (20)$$

3.2.4 Geometric Conditions for MEPaM's Singularities

Let Π_1 be the plane passing through point B_1 and spanned by vectors \underline{u} and \underline{z} . Let Π_3 be the plane passing through point B_3 and spanned by vectors \underline{w} and \underline{z} . Let \mathcal{L}_1 be the intersection line of planes Π_1 and Π_3 . Let \mathcal{L}_2 be the line passing through point B_2 and along \underline{v} . From Eq. (20), MEPaM reaches a parallel singularity if and only if at least one of the two following conditions is verified:

1. The four points of the tetrahedron of corners B_1, B_2, B_3 and \underline{z} are coplanar, namely, the moving platform is vertical as shown in Fig. 6;
2. The lines \mathcal{L}_1 and \mathcal{L}_2 intersect as shown in Fig. 7.

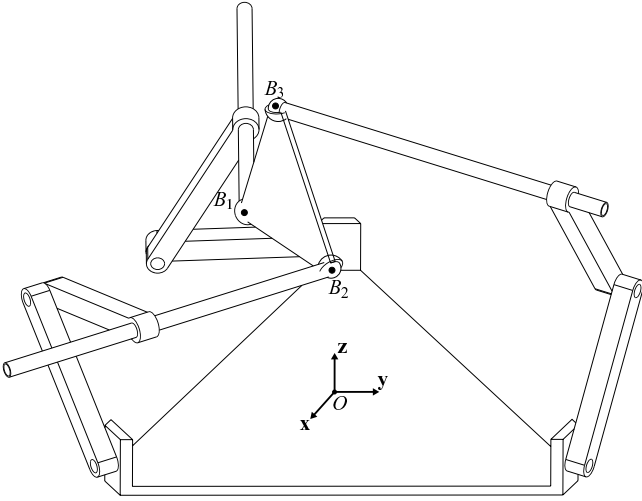


Fig. 6. A singular configuration of MEPaM: its moving platform is vertical

These two conditions yield directly the relation satisfied by the parallel singularities in the orientation workspace, specifically,

$$(-1 + 2Q_2^2 + 2Q_3^2)(Q_2^2 + Q_3^2 + Q_4^2 - 1)Q_4^2 = 0 \quad (21)$$

where variables (Q_2, Q_3, Q_4) , a subset of the quaternions coordinates, represent the orientation space. The quaternions represent the orientation of the moving-platform with a rotation axis \underline{s} and an angle θ . The relation between the quaternions, axis and angle representation can be found in [36]:

$$\begin{aligned} Q_1 &= \cos(\theta/2), \quad Q_2 = s_x \sin(\theta/2) \\ Q_3 &= s_y \sin(\theta/2), \quad Q_4 = s_z \sin(\theta/2) \end{aligned} \quad (22)$$

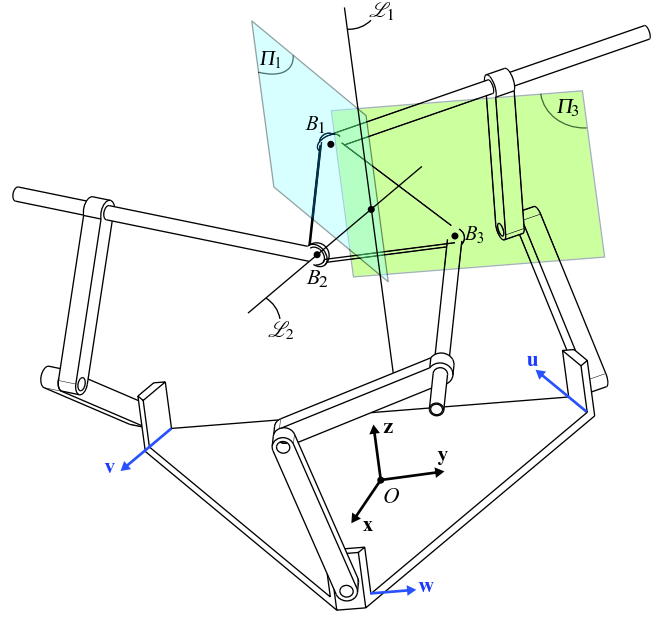


Fig. 7. A singular configuration of MEPaM: lines \mathcal{L}_1 and \mathcal{L}_2 intersect

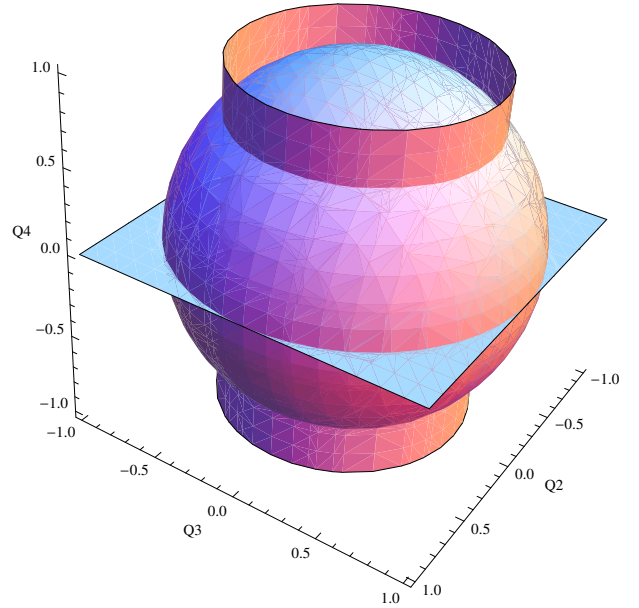


Fig. 8. The parallel singularities of MEPaM in its orientation workspace

where $s_x^2 + s_y^2 + s_z^2 = 1$ and $0 \leq \theta \leq \pi$.

It is evident that Eqn. (21) depends only on the orientation variables (Q_2, Q_3, Q_4) . This means that the parallel singularities do not depend on the position of the centroid of the moving platform. Hence, the parallel singularities of MEPaM can be represented in its orientation workspace only, characterized with the variables (Q_2, Q_3, Q_4) as shown in Fig. 8.

4 Workspace of MEPaM

Due to the mechanical design of MEPaM, the orientation and positional workspaces can be studied separately. Investigations found that the size and shape of the orientation workspace of MEPaM depend only on the orientation of the legs and the physical limitations of the U-joints. The positional workspace can be directly deduced from the possible motions of the epicyclic transmissions.

4.1 Orientation Workspace

The regular orientation workspace of MEPaM was chosen to be $360\text{-}40\text{-}80^\circ$ in a Azimuth, Tilt and Torsion (ϕ, θ, σ) co-ordinate frame, as illustrated in Fig. 9. This workspace was chosen with regards to future use of MEPaM in haptic applications. The U-joints attached to each corner of the platform can only be bent to an angle up to 45° due to physical limitations. The reachable orientation workspace of MEPaM can be calculated by discretizing the orientation workspace and verifying if the two following conditions, which take into account the U-joints angles limitation, are verified for each leg $i = 1, 2, 3$:

$$|\mathbf{y}_i \cdot \mathbf{u}_i| \geq \frac{\sqrt{2}}{2} \quad \text{and} \quad |\mathbf{y}_i \cdot \mathbf{z}_4| \leq \frac{\sqrt{2}}{2} \quad (23)$$

The regular (blue) and reachable (yellow) orientation workspaces of MEPaM are plotted in Fig. 10. It can be seen that the reachable orientation workspace perfectly fits the specified requirements. Moreover, all the orientations that can be reached by the moving platform are singularity-free. This implies that the physical limitations of the U-joints are sufficient in order to not reach a parallel singularity and to stay in the required workspace. Thus, attention to these two points in the control loop of the manipulator need not be considered.

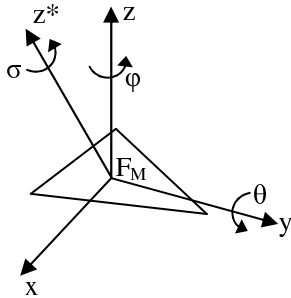


Fig. 9. Co-ordinate frame for Azimuth (ϕ), Tilt (θ) & Torsion (σ) angles [$\phi(z) \rightarrow \theta(y) \rightarrow \sigma(z^*)$]

4.2 Positional Workspace

For symmetrical reasons, the regular positional workspace was defined as a cylinder of diameter and height D_w for the center point of the triangular platform. The

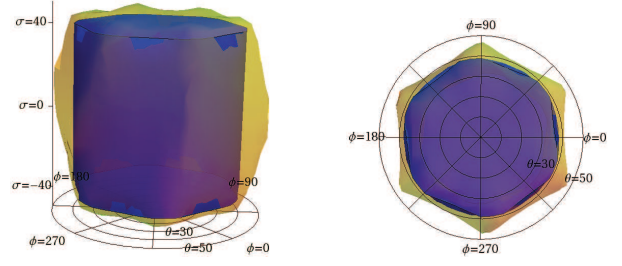


Fig. 10. Regular (blue) and Reachable (yellow) orientation workspaces with respect to the (ϕ, θ, σ) Azimuth, Tilt & Torsion angles

positional requirement of each epicyclic transmission is thus a square of side length D_w , drawn in blue in Fig. 11. However, in order for the device to be able to perform rotations whilst being at a border of the positional workspace, an offset needed to be considered, as shown in red in Fig. 11. Simulation showed that this offset can be approximated by the value of $\frac{3}{8}d_3$. Hence, the positional requirement of each epicyclic transmission is a square of side length $L = D_w + \frac{3}{4}d_3$. The lever arms A and B were then designed in order for MEPaM to have the best accuracy and force capability over its entire workspace.

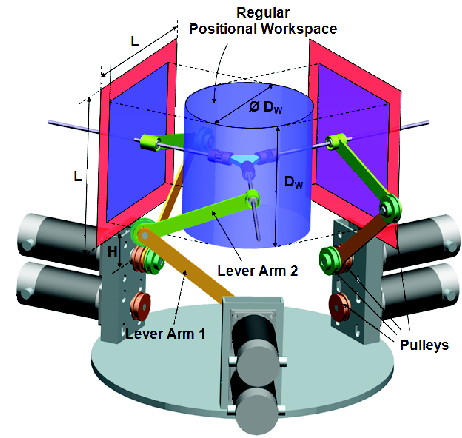


Fig. 11. Regular positional workspace of MEPaM and positional requirements of the epicyclic transmissions

5 Conclusions

A new six-dof epicyclic-parallel manipulator with all actuators mounted on the base, MEPaM, was introduced. The kinematic equations of the manipulator were presented and the singularities analysed. An interesting feature of the manipulator is that the parallel singularity is independent on the position of the end-effector. MEPaM was designed in such a way that the physical limits of the U-joints prevent the end effector from reaching the parallel singularities within its workspace.

Acknowledgments

The authors would like to acknowledge the support of Monash ESGS 2010, the ISL-FAST Program 2010, the French Agence Nationale de la Recherche (Project “SiRoPa”, Singularités des Robots Parallèles), the French Ministry for Foreign Affairs (MAEE) and the French Ministry for Higher Education and Research (MESR) (Project PHC FAST).

References

- [1] Merlet, J., 2006. *Parallel Robots*. Springer, Dordrecht.
- [2] Kong, X., and Gosselin, C., 2007. *Type Synthesis of Parallel Mechanisms*. Springer-Verlag, Berlin.
- [3] Gogu, G., 2008. *Structural Synthesis of Parallel Robots, Part 1: Methodology*. Springer.
- [4] Gogu, G., 2009. *Structural Synthesis of Parallel Robots, Part 2: Translational Topologies with Two and Three Degrees of Freedom*. Springer.
- [5] Clavel, R., 1988. “Delta, a fast robot with parallel geometry”. In Proceedings of the International Symposium on Industrial Robots, pp. 91–100.
- [6] Tsai, L., Walsh, G., and Stamper, R., 1996. “Kinematics of a novel three dof translational platform”. In Proceedings of the 1996 IEEE International Conference on Robotics and Automation, pp. 3446–3451.
- [7] Gregorio, R. D., 2000. “Closed-form solution of the position analysis of the pure translational 3-RUU parallel mechanism”. In Proceedings of the 8th Symposium on Mechanisms and Mechanical Transmissions, pp. 119–124.
- [8] Gosselin, C., 1993. “On the kinematic design of spherical 3-dof parallel manipulators”. *International Journal of Robotics Research*, **12**(4), pp. 394–402.
- [9] Gregorio, R. D., 2001. “Kinematics of a new spherical parallel manipulator with three equal legs: the 3-URC wrist”. *Journal of Robotic Systems*, **18**(5), pp. 213–219.
- [10] Liu, X., Wang, J., and Pritschow, G., 2005. “A new family of spatial 3-dof fully-parallel manipulators with high rotational capability”. *Mechanism and Machine Theory*, **40**(4), pp. 475–494.
- [11] Liu, X., Wang, J., Wu, C., and Kim, J., 2009. “A new family of spatial 3-dof parallel manipulators with two translational and one rotational dofs”. *Robotica*, **27**(2), pp. 241–247.
- [12] Zhao, T., and Huang, Z., 2000. “A novel spatial four-dof parallel mechanism and its position analysis”. *Mechanical Science and Technology*, **19**(6), pp. 927–929.
- [13] Morozov, A., and Angeles, J., 2007. “The mechanical design of a novel Schönflies-motion generator”. *Robotics and Computer-Integrated Manufacturing*, **23**(1), pp. 82–93.
- [14] Huang, Z., and Li, Q. C., 2002. “General methodology for type synthesis of lower mobility symmetrical parallel manipulators and several novel manipulators”. *International Journal of Robotics Research*, **21**(2), pp. 131–146.
- [15] Li, Q., Huang, Z., and Hervé, J., 2004. “Type synthesis of 3R2T 5-dof parallel mechanisms using the Lie group of displacements”. *IEEE Transactions on Robotics and Automation*, **20**(2), pp. 173–180.
- [16] Ben-Horin, P., and Shoham, M., 2006. “Singularity condition of six-degree-of-freedom three-legged parallel robots based on Grassmann-Cayley algebra”. *IEEE Transactions on Robotics*, **22**(4), pp. 577–590.
- [17] Dash, A. K., Chen, I.-M., Yeo, S. H., and Yang, G., 2004. “Instantaneous kinematics and singularity analysis of three-legged parallel manipulators”. *Robotica*, **22**(02), pp. 189–203.
- [18] Behi, F., 1988. “Kinematic analysis for a six-degree-of-freedom 3-PRPS parallel mechanism”. *IEEE Journal of Robotics and Innovation*, **4**(5), pp. 561–565.
- [19] Kohli, D., Lee, S., Tsai, K., and Sandor, G., 1988. “Manipulator configurations based on rotary-linear (r-l) actuators and their direct and inverse kinematics”. *Journal of Mechanisms, Transmissions, and Automation in Design*, **110**(4), pp. 397–404.
- [20] Cleary, K., and Brooks, T., 1993. “Kinematic analysis of a novel 6-dof parallel manipulator”. In IEEE International Conference on Robotics and Automation, pp. 708–713.
- [21] Byun, Y., and Cho, H. S., 1997. “Analysis of a novel 6-dof, 3-PPSP parallel manipulator”. *The International Journal of Robotics Research*, **16**(6), pp. 859–872.
- [22] Simaan, N., Glozman, D., and Shoham, M., 1998. “Design considerations of new six degrees-of-freedom parallel robots”. In IEEE International Conference on Robotics and Automation, pp. 1327–1333.
- [23] Lee, S.-U., and Kim, S., 2006. “Analysis and optimal design of a new 6 dof parallel type haptic device”. In IEEE/RSJ International Conference on Intelligent Robots and Systems, 2006, pp. 460–465.
- [24] Monsarrat, B., and Gosselin, C., 2003. “Workspace analysis and optimal design of a 3-leg 6-dof parallel platform mechanism”. *IEEE Transactions on Robotics and Automation*, **19**(6), December, pp. 954–966.
- [25] Parenti-Castelli, V., and Innocenti, C., 1990. “Direct displacement analysis for some classes of spatial parallel mechanisms”. In Proceedings of the 8th CISM-IFTOMM Symposium on Theory and Practice of Robots and Manipulators, pp. 126–130.
- [26] Angeles, J., 2007. *Fundamentals of Robotic Mechanical Systems: Theory, Methods, and Algorithms*. Springer, New York.
- [27] Gosselin, C., and Angeles, J., 1990. “Singularity analysis of closed-loop kinematic chains”. *IEEE Transactions on Robotics and Automation*, **6**(3), pp. 281–290.
- [28] White, N. L., 1975. “The bracket ring of a combinatorial geometry I”. *Transactions of the American Mathematical Society*, **202**, pp. 79–95.
- [29] White, N. L., 1983. “The bracket of 2-extensors”. *Congressus Numerantium*, **40**, pp. 419–428.
- [30] Kanaan, D., Wenger, P., Caro, S., and Chablat, D., 2009. “Singularity analysis of lower-mobility parallel manipulators using Grassmann-Cayley algebra”. *IEEE Transactions on Robotics*, **25**(5), pp. 995–1004.

- [31] Caro, S., Moroz, G., Gayral, T., Chablat, D., and Chen, C. “Singularity analysis of a six-dof parallel manipulator using Grassmann-Cayley algebra and Gröbner bases”. In *Symposium on Brain, Body and Machine*, Montreal, QC., Canada, November 10-12, 2010.
- [32] Amine, S., Kanaan, D., Caro, S., and Wenger, P., 2010. “Constraint and singularity analysis of lower-mobility parallel manipulators with parallelogram joints”. *Proceedings of the ASME 2010 International Design Engineering Technical Conferences, Montreal, Quebec, Canada*, August 15-18.
- [33] White, N. L., 2005. “Grassmann-Cayley algebra and robotics applications”. *Handbook of Geometric Computing, Part VIII*, pp. 629–656.
- [34] McMillan, T., and White, N., 1991. “The dotted straightening algorithm”. *Journal of Symbolic Computation*, **11**, pp. 471–482.
- [35] Amine, S., Masouleh, M., Caro, S., Wenger, P., and Gosselin, C., 2011. “Singularity analysis of the 4-RUU parallel manipulator based on Grassmann-Cayley algebra and Grassmann geometry”. *Proceedings of the ASME 2011 International Design Engineering Technical Conferences, Washington, DC, USA*, August 28-31.
- [36] Khalil, W., and Dombre, E., 2004. *Modeling, Identification and Control of Robots*. Kogan Page Science.

Appendix A: Direct Kinematics Coefficients

The coefficients of the univariate polynomial Eqn. (8) are:

$$G_4 = 9(A_{1z}^2 - A_{1z}A_{2z} - A_{1z}A_{3z} + A_{2z}^2 - A_{2z}A_{3z} + A_{3z}^2)^2$$

$$\begin{aligned}
G_3 = & 12\sqrt{3}A_{1x}A_{2z}^4 - 12\sqrt{3}A_{1z}^4A_{2x} - 12\sqrt{3}A_{1x}A_{3z}^4 \\
& + 12\sqrt{3}A_{1z}^4A_{3x} - 24\sqrt{3}A_{2x}A_{3z}^4 + 24\sqrt{3}A_{2z}^4A_{3x} \\
& - 6\sqrt{3}A_{1z}^4d_0 - 24\sqrt{3}A_{2z}^4d_0 + 12\sqrt{3}A_{3z}^4d_0 \\
& + 66\sqrt{3}A_{1z}A_{2z}^3d_0 + 48\sqrt{3}A_{1z}^3A_{2z}d_0 \\
& - 42\sqrt{3}A_{1z}A_{3z}^3d_0 - 24\sqrt{3}A_{1z}^3A_{3z}d_0 \\
& - 6\sqrt{3}A_{2z}A_{3z}^3d_0 + 30\sqrt{3}A_{2z}^3A_{3z}d_0 \\
& + 36\sqrt{3}A_{1x}A_{1z}^2A_{2z}^2 - 36\sqrt{3}A_{1x}A_{1z}^2A_{3z}^2 \\
& - 72\sqrt{3}A_{1z}^2A_{2x}A_{3z}^2 + 72\sqrt{3}A_{1z}^2A_{2z}^2A_{3x} \\
& - 36\sqrt{3}A_{2x}A_{2z}^2A_{3z}^2 + 36\sqrt{3}A_{2z}^2A_{3x}A_{3z}^2 \\
& - 72\sqrt{3}A_{1z}^2A_{2z}^2d_0 + 36\sqrt{3}A_{1z}^2A_{3z}^2d_0 \\
& - 18\sqrt{3}A_{2z}^2A_{3z}^2d_0 - 18\sqrt{3}A_{1x}A_{2z}^2d_3^2 \\
& + 18\sqrt{3}A_{1x}A_{3z}^2d_3^2 - 18\sqrt{3}A_{2x}A_{2z}^2d_3^2 \\
& + 18\sqrt{3}A_{2x}A_{3z}^2d_3^2 - 18\sqrt{3}A_{2z}^2A_{3x}d_3^2 \\
& + 18\sqrt{3}A_{3x}A_{3z}^2d_3^2 + 27\sqrt{3}A_{2z}^2d_0d_3^2 \\
& - 27\sqrt{3}A_{3z}^2d_0d_3^2 - 36\sqrt{3}A_{1x}A_{1z}A_{2z}^3 \\
& - 24\sqrt{3}A_{1x}A_{1z}^3A_{2z} + 36\sqrt{3}A_{1x}A_{1z}A_{3z}^3 \\
& + 24\sqrt{3}A_{1x}A_{1z}^3A_{3z} - 12\sqrt{3}A_{1z}A_{2x}A_{2z}^3 \\
& + 12\sqrt{3}A_{1x}A_{2z}A_{3z}^3 - 12\sqrt{3}A_{1x}A_{2z}^3A_{3z}
\end{aligned}$$

$$\begin{aligned}
& + 60\sqrt{3}A_{1z}A_{2x}A_{3z}^3 - 60\sqrt{3}A_{1z}A_{2z}^3A_{3x} \\
& + 48\sqrt{3}A_{1z}^3A_{2x}A_{3z} - 48\sqrt{3}A_{1z}^3A_{2z}A_{3x} \\
& + 12\sqrt{3}A_{1z}A_{3x}A_{3z}^3 + 36\sqrt{3}A_{2x}A_{2z}A_{3z}^3 \\
& + 12\sqrt{3}A_{2x}A_{2z}^3A_{3z} - 12\sqrt{3}A_{2z}A_{3x}A_{3z}^3 \\
& - 36\sqrt{3}A_{2z}^3A_{3x}A_{3z} - 36\sqrt{3}A_{1x}A_{1z}A_{2z}A_{3z}^2 \\
& + 36\sqrt{3}A_{1x}A_{1z}A_{2z}^2A_{3z} - 36\sqrt{3}A_{1z}A_{2x}A_{2z}A_{3z}^2 \\
& + 36\sqrt{3}A_{1z}A_{2x}A_{2z}^2A_{3z} - 36\sqrt{3}A_{1z}A_{2z}A_{3x}A_{3z}^2 \\
& + 36\sqrt{3}A_{1z}A_{2z}^2A_{3x}A_{3z} + 54\sqrt{3}A_{1z}A_{2z}A_{3z}^2d_0 \\
& - 54\sqrt{3}A_{1z}A_{2z}^2A_{3z}d_0 + 36\sqrt{3}A_{1x}A_{1z}A_{2z}d_3^2 \\
& - 36\sqrt{3}A_{1x}A_{1z}A_{3z}d_3^2 + 36\sqrt{3}A_{1z}A_{2x}A_{2z}d_3^2 \\
& - 36\sqrt{3}A_{1z}A_{2x}A_{3z}d_3^2 + 36\sqrt{3}A_{1z}A_{2z}A_{3x}d_3^2 \\
& - 36\sqrt{3}A_{1z}A_{3x}A_{3z}d_3^2 - 54\sqrt{3}A_{1z}A_{2z}d_0d_3^2 \\
& + 54\sqrt{3}A_{1z}A_{3z}d_0d_3^2
\end{aligned}$$

$$\begin{aligned}
G_2 = & a_{01}^2 - a_{01}a_{10} - a_{01}a_{11}b_{10} - 2a_{01}a_{20}b_{01} + 6a_{00}b_{10}^2 \\
& + 2a_{01}a_{20}b_{10} - 2a_{01}a_{21}b_{00} + a_{01}a_{21}b_{10}^2 - 4a_{00}b_{00} \\
& + 3a_{01}a_{30}b_{00} + 3a_{01}a_{30}b_{01}b_{10} - 3a_{01}a_{30}b_{10}^2 \\
& - 3a_{01}b_{00}b_{10} + a_{01}b_{10}^3 + 4a_{01}b_{00}b_{01} + 4a_{01}b_{10}^3 \\
& - 8a_{01}b_{00}b_{10} - 4a_{01}b_{01}b_{10}^2 + a_{10}^2 + 2a_{10}a_{11}b_{01} \\
& - a_{10}a_{20}b_{01} - a_{10}a_{20}b_{10} - a_{10}a_{21}b_{00} - a_{10}a_{21}b_{01}b_{10} \\
& + a_{10}a_{30}b_{00} - 4a_{10}a_{30}b_{00} - 2a_{10}a_{30}b_{01}^2 + 4a_{10}b_{00}b_{01} \\
& + a_{10}a_{30}b_{10}^2 - 2a_{10}b_{00}b_{10} + 2a_{10}a_{30}b_{01}b_{10} - a_{10}b_{01}b_{10}^2 \\
& + 6a_{10}b_{00}b_{01} - 3a_{10}b_{00}b_{10} + 6a_{10}b_{00}b_{10} + 3a_{10}b_{01}^2b_{10} \\
& - 3a_{10}b_{01}b_{10}^2 - a_{10}b_{10}^3 + 2a_{12}a_{10}b_{00} - a_{02}a_{10}b_{10} \\
& + a_{11}^2b_{00} - a_{11}a_{20}b_{00} - a_{11}a_{20}b_{01}b_{10} - a_{11}a_{21}b_{00}b_{10} \\
& - 4a_{11}a_{30}b_{00}b_{01} + 2a_{11}a_{30}b_{00}b_{10} + 2a_{11}b_{00}^2 - a_{00}a_{11} \\
& + a_{11}a_{30}b_{01}b_{10}^2 - a_{11}b_{00}b_{10}^2 - a_{11}b_{01}b_{10}^3 + 2a_{20}^2b_{00} \\
& + 3a_{11}b_{00}^2 + 6a_{11}b_{00}b_{01}b_{10} - 3a_{11}b_{00}b_{10}^2 + a_{20}^2b_{01}^2 \\
& + 4a_{20}a_{21}b_{00}b_{01} - 2a_{20}a_{30}b_{00}b_{01} - 2a_{20}a_{30}b_{00}b_{10} \\
& - a_{20}a_{30}b_{01}^2b_{10} + a_{20}b_{00}^2 + 2a_{20}b_{00}b_{01}b_{10} + a_{20}b_{00}^2 \\
& - 6a_{20}b_{00}^2 - 6a_{20}b_{00}b_{01}^2 + 4a_{20}b_{00}b_{01}b_{10} + 2a_{20}b_{00}b_{10}^2 \\
& + a_{20}b_{01}^2b_{10}^2 - a_{12}a_{20}b_{00}b_{10} - 2a_{02}a_{20}b_{00} - 2a_{00}a_{20} \\
& + a_{02}a_{20}b_{10}^2 + a_{00}a_{20} - 2a_{21}a_{30}b_{00}b_{01}b_{10} + a_{21}^2b_{00}^2 \\
& - a_{21}a_{30}b_{00}^2 + a_{21}b_{00}^2b_{10} - 6a_{21}b_{00}^2b_{01} + 2a_{21}b_{00}^2b_{10} \\
& + 2a_{21}b_{00}b_{01}b_{10}^2 - 2a_{00}a_{21}b_{01} + 2a_{00}a_{21}b_{10} + 3a_{30}^2b_{00}^2 \\
& + 3a_{30}^2b_{00}b_{01}^2 - 6a_{30}b_{00}^2b_{01} - 3a_{30}b_{00}^2b_{01} - 4a_{00}b_{10}^2 \\
& - 3a_{30}b_{00}^2b_{10} - 3a_{30}b_{00}b_{01}^2b_{10} - a_{00}a_{12}b_{10} + 2a_{00}a_{02} \\
& - 2a_{12}a_{30}b_{00}^2 + a_{12}a_{30}b_{00}b_{10}^2 + 3a_{02}a_{30}b_{00}b_{10} + 4b_{00}^3 \\
& + 3a_{00}a_{30}b_{01} - a_{02}a_{30}b_{10}^3 - 3a_{00}a_{30}b_{10} + 3a_{00}a_{30}b_{10} \\
& + 2b_{00}^3 + 3b_{00}^2b_{01}b_{10} - 3a_{00}b_{00} - 3a_{00}b_{01}b_{10} + 3a_{00}b_{10}^2 \\
& + 6b_{00}^2b_{01}^2 + 3a_{12}b_{00}^2b_{10} + 2a_{02}b_{00}^2 + 4a_{00}b_{00} + a_{02}b_{10}^4 \\
& + 2a_{00}b_{01}^2 - a_{12}b_{00}b_{10}^3 - 4a_{02}b_{00}b_{10}^2 - 8a_{00}b_{01}b_{10}
\end{aligned}$$

$$\begin{aligned}
G_1 = & b_{01}a_{10}^2 - a_{10}a_{20}b_{00} - b_{01}a_{10}a_{20}b_{10} + 2a_{10}a_{30}b_{00}b_{10} \\
& - 4b_{01}a_{10}a_{30}b_{00} + b_{01}a_{10}a_{30}b_{10}^2 + 3a_{10}b_{00}^2 - b_{01}a_{10}b_{10}^3 \\
& - 3a_{10}b_{00}b_{10}^2 + 6b_{01}a_{10}b_{00}b_{10} + 2a_{10}b_{00}^2 - a_{10}b_{00}b_{10}^2 \\
& - a_{21}a_{10}b_{00}b_{10} + 2a_{11}a_{10}b_{00} - a_{01}a_{10}b_{10} - a_{00}a_{10} \\
& + 2b_{01}a_{20}^2b_{00} - a_{20}a_{30}b_{00}^2 - 2b_{01}a_{20}a_{30}b_{00}b_{10} - a_{30}b_{00}^3 \\
& + 2a_{20}b_{00}^2b_{10} - 6b_{01}a_{20}b_{00}^2 + 2b_{01}a_{20}b_{00}b_{10}^2 + 2a_{00}a_{01} \\
& + a_{20}b_{00}^2b_{10} + 2a_{21}a_{20}b_{00}^2 - a_{11}a_{20}b_{00}b_{10} - 2a_{00}b_{01}a_{20} \\
& - 2a_{01}a_{20}b_{00} + a_{01}a_{20}b_{10}^2 + 2a_{00}a_{20}b_{10} + 3b_{01}a_{30}^2b_{00}^2 \\
& - 3b_{01}a_{30}b_{00}^2b_{10} - 2a_{30}b_{00}^3 - a_{21}a_{30}b_{00}^2b_{10} + b_{00}^3b_{10} \\
& - 2a_{11}a_{30}b_{00}^2 + a_{11}a_{30}b_{00}b_{10}^2 + a_{00}b_{10}^3 + 4b_{01}^2b_{00}^3 \\
& + 3a_{00}a_{30}b_{00} - a_{01}a_{30}b_{10}^3 - 3a_{00}a_{30}b_{10}^2 + 3a_{01}a_{30}b_{00}b_{10} \\
& + 3a_{00}b_{01}a_{30}b_{10} - 2a_{21}b_{00}^3 + a_{21}b_{00}^2b_{10}^2 + 3a_{11}b_{00}^2b_{10} \\
& + 2a_{01}b_{00}^2 - a_{11}b_{00}b_{10}^3 - 4a_{01}b_{00}b_{10}^2 + 4a_{00}b_{01}b_{00} \\
& - 8a_{00}b_{00}b_{10} + a_{01}b_{10}^4 - 4a_{00}b_{01}b_{10}^2 - 3a_{00}b_{00}b_{10} \\
& + 4a_{00}b_{10}^3 - 2a_{00}a_{21}b_{00} + a_{00}a_{21}b_{10}^2 - a_{00}a_{11}b_{10}
\end{aligned}$$

$$\begin{aligned}
c_{00} = & A_{2x}^2 + A_{2x}A_{3x} - 2A_{2x}d_0 + A_{2z}^2 - 2A_{2z}A_{3z} + A_{3x}^2 \\
& - A_{3x}d_0 + A_{3z}^2 + d_0^2 - d_3^2 \\
c_{01} = & -\sqrt{3}A_{3x} \\
c_{10} = & \sqrt{3}A_{2x} - \sqrt{3}d_0 \\
d_{00} = & A_{1x}^2 + A_{1x}A_{3x} - A_{1x}d_0 + A_{1z}^2 - 2A_{1z}A_{3z} + A_{3x}^2 \\
& - 2A_{3x}d_0 + A_{3z}^2 + d_0^2 - d_3^2 \\
d_{01} = & \sqrt{3}A_{3x} - \sqrt{3}d_0 \\
d_{10} = & -\sqrt{3}A_{1x}
\end{aligned}$$

$$\begin{aligned}
G_0 = & a_{00}^2 - a_{00}a_{10}b_{10} - 2a_{00}a_{20}b_{00} + a_{00}a_{20}b_{10}^2 + a_{00}b_{10}^4 \\
& + 3a_{00}a_{30}b_{00}b_{10} - a_{00}a_{30}b_{10}^3 + 2a_{00}b_{00}^2 - a_{30}b_{00}^3b_{10} \\
& - 4a_{00}b_{00}b_{10}^2 - a_{10}a_{20}b_{00}b_{10} - 2a_{10}a_{30}b_{00}^2 + a_{20}b_{00}^2b_{10}^2 \\
& + 3a_{10}b_{00}^2b_{10} + a_{10}a_{30}b_{00}b_{10}^2 - a_{10}b_{00}b_{10}^3 + a_{20}^2b_{00}^2 \\
& - a_{20}a_{30}b_{00}^2b_{10} - 2a_{20}b_{00}^3 + a_{30}^2b_{00}^3 + a_{10}^2b_{00} + b_{00}^4
\end{aligned}$$

where

$$\begin{aligned}
a_{00} = & c_{00}^2 - c_{00}c_{10}d_{10} - 2c_{00}d_{00} + c_{00}d_{10}^2 + c_{10}^2d_{00} \\
& - c_{10}d_{00}d_{10} + d_{00}^2 \\
a_{01} = & 2d_{00}d_{01} + c_{10}^2d_{01} - c_{00}c_{10} - 2c_{00}d_{01} + 2c_{00}d_{10} \\
& - c_{10}d_{00} - c_{10}d_{01}d_{10} \\
a_{02} = & c_{10}^2 - c_{10}d_{01} - d_{10}c_{10} + d_{01}^2 + 2d_{00} + c_{00} - 2c_{00} \\
a_{03} = & 2d_{01} - c_{10} \\
a_{10} = & 2c_{00}c_{01} + c_{01}d_{10}^2 - c_{00}d_{10} - c_{01}c_{10}d_{10} - 2c_{01}d_{00} \\
& + 2c_{10}d_{00} - d_{00}d_{10} \\
a_{11} = & 2c_{01}d_{10} - c_{01}c_{10} - 2c_{01}d_{01} - c_{00} + 2c_{10}d_{01} - d_{00} \\
& - d_{01}d_{10} \\
a_{12} = & c_{01} - d_{01} - 2c_{01} + 2c_{10} - d_{10} \\
a_{20} = & c_{01}^2 - c_{01}d_{10} + d_{00} + d_{10}^2 - c_{10}d_{10} + 2c_{00} - 2d_{00} \\
a_{21} = & d_{01} - c_{01} - c_{10} - 2d_{01} + 2d_{10} \\
a_{30} = & 2c_{01} - d_{10} \\
b_{00} = & A_{1x}^2 + A_{1x}A_{2x} - 2A_{1x}d_0 + A_{1z}^2 - 2A_{1z}A_{2z} + A_{2x}^2 \\
& - A_{2x}d_0 + A_{2z}^2 + d_0^2 - d_3^2 \\
b_{01} = & -\sqrt{3}A_{2x} \\
b_{10} = & \sqrt{3}A_{1x} - \sqrt{3}d_0
\end{aligned}$$